water

MDPI

Article

Thermodynamic and Microbubble-Dynamics Framework for Dissolved-Air Flotation Pretreatment of Arsenic-Rich Groundwater

Zorana Radibratović [1], Biljana Cakić [1], Mirjana Kijevčanin [2], Ivona Radović [2], David Mitrinović [1] and Marija Perović [1,*]

[1] Jaroslav Černi Water Institute, 11226 Belgrade, Serbia; zorana.radibratovic@jcerni.rs (Z.R.); biljana.cakic@jcerni.rs (B.C.); david.mitrinovic@jcerni.rs (D.M.)
[2] Faculty of Technology and Metallurgy, University of Belgrade, 11000 Belgrade, Serbia; mirjana@tmf.bg.ac.rs (M.K.); ivonag@tmf.bg.ac.rs (I.R.)
* Correspondence: marija.perovic@jcerni.rs

Abstract

Dissolved-air flotation (DAF) is widely used for surface-water pretreatment but remains insufficiently explored for chemically complex groundwater. This study develops a thermodynamic and bubble-dynamics modeling framework to evaluate the feasibility of DAF pretreatment for groundwater containing elevated arsenic, natural organic matter (NOM), and color. The study is theoretical and model-based; no experimental dissolved-air flotation tests were performed. Air solubility was calculated at pressures of 4–6 bar and temperatures of 13–17 °C, while microbubble size, rise velocity, and bubble–floc interaction efficiencies were estimated using established physical models. Laboratory coagulation–flocculation jar tests with $FeCl_3$ and $FeCl_3$/PAC were used to define realistic floc properties prior to flotation modeling. No experimental dissolved-air flotation tests were conducted; all flotation-related results presented in this study are derived from thermodynamic and hydrodynamic modeling. Results show that a temperature decrease from 17 to 13 °C increases effective gas supersaturation by ~15% and shifts predicted microbubble diameters from ~60–90 µm to ~35–60 µm under identical operating conditions. The qualitative consistency between modeled flotation-relevant parameters and previously observed coagulation–flocculation trends for color, total organic carbon, and arsenic removal supports the proposed mechanistic framework. The study demonstrates how coupling coagulation chemistry with thermodynamically optimized air dissolution can enhance DAF applicability for arsenic- and NOM-rich groundwater.

Keywords: dissolved-air flotation; groundwater; thermos-dynamics; microbubble dynamics; coagulation–flocculation

Academic Editor: Christos S. Akratos

Received: 12 February 2026
Revised: 3 March 2026
Accepted: 5 March 2026
Published: 7 March 2026

1. Introduction

Groundwater represents the dominant freshwater resource on Earth, accounting for more than 97% of global freshwater reserves (excluding glaciers and ice-covered regions) and serves as the primary source of drinking water for approximately 75% of the population in both the European Union and the Republic of Serbia [1,2]. Considering the critical reliance on groundwater as a primary drinking-water source, ensuring its adequate quality and treatability represents an important challenge, particularly in aquifers characterized by elevated concentrations of naturally occurring contaminants. Groundwater sources with

elevated arsenic, natural organic matter, and color pose a significant challenge for drinking-water production, as the presence of organic metal complexes and colloidal constituents reduce the efficiency of conventional pretreatment processes. DAF is widely applied in the treatment of surface water and wastewater, while its application to groundwater remains largely unexplored. The limited available literature focuses primarily on empirical performance results, while the mechanistic basis governing bubble formation, gas dissolution, and bubble–floc interactions in groundwater remains insufficiently explored [3,4]. Bubble formation, nucleation, and hydrodynamics have been extensively studied in flotation systems [4–6] but rarely applied to low-turbidity groundwater.

DAF operates by dissolving air in water under pressure and releasing it to generate microbubbles capable of attaching to coagulated particles and transporting them to the surface. The efficiency of this process depends on several interrelated steps: gas dissolution, supersaturation, bubble nucleation, bubble size distribution, and the attachment of bubbles to flocs formed during coagulation and flocculation. Each of these steps is governed by thermodynamic and hydrodynamic principles that determine the number, size, and stability of bubbles produced during depressurization. Gas solubility under pressure is governed by Henry's law and strongly depends on temperature [7,8]. Floc characteristics have a major effect on bubble attachment, as predicted by classical collision and adhesion theories [9,10].

Groundwater characteristics differ substantially from surface waters characteristics, directly influencing DAF performance. Lower temperatures typical of deep aquifers affect gas solubility and bubble nucleation. Higher concentrations of dissolved gases such as methane influence supersaturation behavior. The low content of suspended solids results in fewer naturally available attachment sites for bubbles, making the properties of coagulated flocs especially important. In groundwater containing arsenic, most of the arsenic is associated with dissolved species that require oxidation and coagulation before effective flotation can occur [11,12]. These specific conditions emphasize the need for a mechanistic understanding of how thermodynamic parameters and bubble dynamics impact the efficiency of DAF pretreatment. Several alternative technologies are available for arsenic removal from groundwater, including adsorption onto iron-based media, ion exchange, membrane filtration (e.g., reverse osmosis or nanofiltration), and advanced oxidation–filtration combinations. While these approaches can achieve high removal efficiencies, their implementation may involve site-specific operational considerations such as membrane fouling, concentrate management, media regeneration requirements, or increased chemical demand, particularly in the presence of elevated natural organic matter (NOM). In groundwater systems where arsenic is effectively converted to particulate or co-precipitated forms through coagulation, dissolved-air flotation offers a physically distinct separation mechanism based on bubble-assisted transport rather than surface filtration or mass transfer to a sorbent. Under such conditions, DAF may provide advantages as a pretreatment step by reducing filter loading, enhancing removal of low-density flocs, and improving operational robustness under cold-temperature conditions typical of deep aquifers.

Recent laboratory pretreatment studies on groundwater from Zrenjanin, Serbia, demonstrated that optimized coagulant combinations, particularly $FeCl_3$ and polyaluminum chloride (PAC), significantly improve the removal of color, total organic carbon, and particulate-bound arsenic [13]. By effectively transferring these contaminants from the dissolved to the particulate phase, these findings indicate that subsequent separation processes such as dissolved-air flotation may be particularly suitable as pretreatment steps for this groundwater. The interpretation of these results has so far been mainly empirical, without a detailed thermodynamic evaluation of gas dissolution behavior or a quantitative assessment of bubble–floc interactions.

Gas solubility was calculated for pressures of 4–6 bar and temperatures of 13–17 °C, corresponding to realistic DAF operating conditions and the measured seasonal temperature range of the Zrenjanin groundwater source [13,14]. This parameter range was selected to capture the combined influence of pressure and temperature on gas supersaturation and microbubble formation under conditions relevant to full-scale groundwater pretreatment. Bubble size distribution, terminal rise velocity, and attachment efficiency to $FeCl_3$/PAC-induced flocs were evaluated using established physical models and interpreted in the context of trends observed in laboratory coagulation–flocculation pretreatment tests. By integrating theoretical predictions with experimentally derived floc characteristics, this study provides a mechanistic basis for assessing DAF pretreatment feasibility and for interpreting how thermodynamic conditions and microbubble behavior may influence flotation-relevant interactions in chemically complex groundwater systems. Despite extensive application of dissolved-air flotation in surface-water treatment, its mechanistic evaluation for chemically complex groundwater systems remains limited. Previous studies have predominantly focused on empirical performance indicators, while the combined influence of thermodynamic gas dissolution, microbubble dynamics, and coagulation-induced floc properties has not been systematically addressed for arsenic-rich groundwater matrices. The present study addresses this gap by developing an integrated mechanistic framework that couples (a) temperature-dependent gas solubility and supersaturation modeling, (b) microbubble size and rise-velocity estimation, and (c) bubble–floc collision and attachment analysis under groundwater-specific chemical conditions. In addition, a groundwater-specific baseline dissolved-gas definition is introduced, accounting for strongly reducing source conditions rather than assuming equilibrium with atmospheric air.

The present work constitutes a theoretical thermodynamic–hydrodynamic modeling study aimed at the mechanistic interpretation and feasibility screening of DAF pretreatment under groundwater-specific conditions. It does not report experimental flotation performance but rather develops a physically grounded framework integrating gas dissolution thermo-dynamics with bubble-dynamics and collision–attachment modeling.

The modeling framework developed herein is intended as a feasibility-screening and pre-design analytical tool for groundwater DAF systems operating at pilot or full scale, rather than as a validated performance prediction model. The objective is not to simulate a specific laboratory apparatus, but rather to evaluate thermodynamic and hydrodynamic operating windows under realistic process conditions typical of drinking-water DAF installations.

2. Materials and Methods

2.1. Model Type and Scope

This study adopts a theoretical thermodynamic–hydrodynamic modeling approach that integrates: (a) gas-dissolution and supersaturation calculations based on Henry's law with temperature correction; (b) hydrodynamic estimation of microbubble size and terminal rise velocity; and (c) analytical modeling of bubble–floc collision and attachment efficiencies.

No laboratory or pilot-scale dissolved-air flotation (DAF) experiments were conducted within this study. Previously reported coagulation–flocculation jar tests were used exclusively to define representative floc boundary conditions (e.g., floc size range and coagulation regime) serving as input parameters for the modeling framework, rather than to validate flotation removal performance.

The reported flotation-related results (gas solubility, effective supersaturation, bubble-size ranges, rise velocities, and interaction efficiencies) therefore represent scenario-based estimates intended to evaluate relative trends and operating windows under realistic groundwater conditions, rather than quantitatively validated predictions of full-scale DAF

performance. Bubble size is treated parametrically in accordance with DAF design guidance, reflecting its dependence on thermodynamic driving force and release/coalescence conditions rather than direct measurement in the present study.

Figure 1 schematically illustrates the modeled DAF process elements and data linkages used in this study. The diagram shows how jar-test coagulation–flocculation defines floc-related boundary conditions, how pressurized recycle water dissolves air in the saturator, and how rapid pressure release generates microbubbles in the contact zone. Bubble–floc collision and attachment processes are represented conceptually within the modeling framework, followed by agglomerate rise and separation in the flotation tank. Bubble size is evaluated using ranges consistent with DAF design guidance due to its dependence on release and coalescence conditions, and the schematic indicates that coalescence may increase bubble diameters between the contact and separation zones.

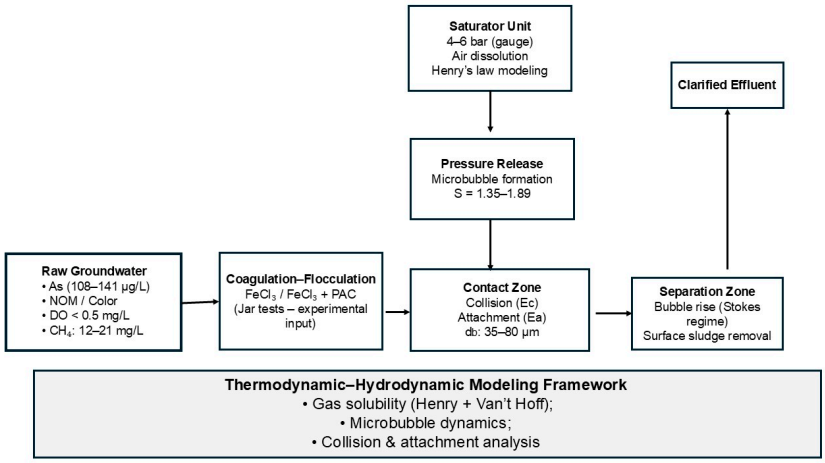

Figure 1. Conceptual configuration of the DAF system represented in the thermodynamic–hydrodynamic modeling framework. Coagulation–flocculation experiments provide floc-related input parameters, while gas dissolution, microbubble formation, bubble rise velocity, and bubble–floc interaction processes are evaluated analytically under pilot- and full-scale representative operating conditions.

2.2. Groundwater Characteristics

Arsenic-rich groundwater represents a major drinking-water challenge in many parts of the world, including South and Southeast Asia, Central Europe, and regions of North and South America. In these settings, naturally occurring arsenic is commonly associated with reducing aquifer conditions and elevated concentrations of NOM. Groundwater under such conditions often exhibits pronounced color, low dissolved oxygen, sometimes elevated methane concentrations, and complex geogenic organic matter, all of which complicate conventional treatment processes and increase coagulant demand. These hydrogeochemical characteristics are not region-specific but are typical of deep, reducing aquifers in sedimentary basins, where arsenic mobilization is coupled with NOM release and distinctive gas-solubility behavior. Consequently, the simultaneous presence of arsenic, color, and NOM represents a widespread treatment challenge that motivates the evaluation of advanced pretreatment strategies capable of addressing multiple water-quality constraints.

In Serbia, particularly in the Autonomous Province of Vojvodina (APV), groundwater used for drinking-water supply is frequently characterized by elevated arsenic concentrations, pronounced natural color, and high levels of NOM, reflecting the complex hydrogeochemical conditions of the Pannonian Basin. Arsenic contamination is a long-standing environmental and public-health concern in northern Serbia, particularly in the APV, where groundwater arsenic concentrations frequently exceed the WHO guideline value of 10 µg/L and may reach tens to several hundred micrograms per liter [15–17].

Drinking-water regulations in Serbia, the European Union, and the United States uniformly adopt a maximum allowable concentration of 10 µg/L for arsenic [18–20].

Because public water supply in APV relies almost exclusively on groundwater, the combined presence of arsenic, color, and NOM represents a regionally significant treatment challenge and motivates the evaluation of advanced pretreatment strategies capable of solving multiple water-quality constraints simultaneously.

The groundwater considered in this study originates from the municipal wellfield supplying the city of Zrenjanin (Vojvodina, Serbia), a location with a well-documented, decades-long drinking-water-quality problem related to increased arsenic and organic matter content in groundwater. Groundwater temperature typically ranges from 13 to 17 °C, while dissolved oxygen concentrations are generally below 0.5 mg/L and dissolved methane concentrations range from 12 to 21 mg/L [13]. These reducing hydrochemical conditions are representative of deep aquifers in the Pannonian Basin and strongly influence gas solubility, supersaturation behavior, and microbubble formation during pressurization and depressurization. For this reason, Zrenjanin groundwater was selected as a representative case study for thermodynamic and bubble-dynamics modeling of DAF under realistic operating conditions.

Because the efficiency of dissolved-air flotation strongly depends on the size, density, and surface properties of pre-formed flocs, representative coagulation–flocculation conditions must be defined prior to flotation modeling.

The Conceptual DAF System Modeled represents a conventional dissolved-air flotation configuration consisting of: (a) a saturator unit operating at 4–6 bar gauge pressure for air dissolution, (b) a pressure-release mechanism enabling rapid depressurization and microbubble formation, (c) a contact zone where bubble–floc interactions occur, and (d) a separation zone allowing buoyant transport and surface skimming.

The thermodynamic and hydrodynamic calculations were performed using operating parameters consistent with full-scale drinking-water DAF units and laboratory DAF jar testers. The framework is therefore intended to reflect practical pilot- and field-scale conditions rather than purely idealized laboratory microreactors.

2.3. Definition of Coagulation–Flocculation Conditions for DAF Modeling

Jar-test data from four laboratory-test series (JAR 1–JAR 4), previously reported [13] and conducted on groundwater from the municipal wellfield supplying the city of Zrenjanin, were used in this study to define representative coagulation–flocculation conditions and corresponding floc-related parameters required for subsequent DAF modeling. No laboratory-scale, pilot-scale, or full-scale dissolved-air flotation unit was operated within the scope of this study. The jar tests were conducted exclusively to characterize coagulation behavior and to define representative floc-related boundary conditions for subsequent thermodynamic and bubble-dynamics modeling. Conducted jar tests encompassed a broad range of coagulant configurations, including ferric chloride ($FeCl_3$) applied alone, pre-oxidation with sodium hypochlorite (NaOCl), combining $FeCl_3$ and polyaluminum chloride (PAC) dosing, and selected variations in coagulant ratios and auxiliary polymers. Based on the consistent trends observed across JAR 1-JAR 4, coagulation conditions involving combined $FeCl_3$ and PAC dosing were adopted to define the floc-related boundary conditions for DAF modeling. These conditions were used to establish representative ranges of floc size, density, and surface interaction properties applied as input parameters in the thermodynamic and bubble-dynamics modeling framework.

2.4. Thermodynamic Model for Gas Dissolution

Gas dissolution under pressurized conditions was described using Henry's law, with temperature dependence accounted for through the Van't Hoff relationship [7,8] (Equation (1)). The degree of supersaturation required for microbubble nucleation in DAF systems has been discussed in earlier flotation studies [3,4,21,22].

$$C = k_H \cdot p \quad (1)$$

where C is the dissolved-gas concentration (mol/L); k_H is Henry's constant corrected for; temperature; and p is the partial pressure of air, calculated from the absolute operating pressure assuming atmospheric air composition.

For air, Henry's constant was adjusted using the Van't Hoff temperature dependence (Equation (2)):

$$k_H(T) = k_H(T_0)\exp\left[\frac{-\Delta H}{R}\left(\frac{1}{T} - \frac{1}{T_0}\right)\right] \quad (2)$$

where ΔH is the enthalpy of dissolution; R is the gas constant; and T the water temperature (K).

Calculations were performed for pressures of 4 and 6 bar and temperatures of 13 and 17 °C, representing realistic DAF operating conditions at the groundwater source. The operating pressures reported (4 and 6 bar) refer to gauge pressure measured at the saturator; absolute pressures used in thermodynamic calculations were obtained by adding atmospheric pressure (1 bar).

The effective supersaturation in the flotation jar was calculated using the recycle ratio (R), defined as the ratio of pressurized whitewater volume to the effective jar volume, in accordance with the manufacturer's DAF jar-test procedure [14].

Because the raw groundwater is characterized by strongly reducing conditions (DO < 0.5 mg/L) and elevated methane concentrations (12–21 mg/L), it cannot be assumed to be equilibrated with atmospheric air. In dissolved-air flotation systems, the gas phase introduced into the saturator consists of atmospheric air under controlled pressure. Consequently, only the components of the injected gas phase (primarily N_2, O_2, and Ar) participate in the pressurization–depressurization equilibrium described by Henry's law.

Methane present in the raw groundwater originates from in situ biogeochemical processes under reducing aquifer conditions and is not part of the injected gas phase. Because no methane gas-phase partial pressure was imposed in the saturator, methane cannot be treated within the same thermodynamic equilibrium framework used to calculate dissolved-air supersaturation. Its concentration therefore does not contribute to the supersaturation driving force generated during depressurization of pressurized whitewater.

For this reason, the baseline dissolved-air concentration prior to pressurization was defined using only atmospheric gas components (N_2 and Ar at equilibrium at 1 bar and measured dissolved oxygen), while methane was treated separately as an indicator of redox state rather than as a contributor to DAF supersaturation potential (Equation (3)):

$$C_{ambient} = C^*_{N_2}(\mathrm{T}, 1\ \mathrm{bar}) + C^*_{Ar}(\mathrm{T}, 1\ \mathrm{bar}) + C_{O_2,\mathrm{meas}} \quad (3)$$

Here, $C^*_{N_2}$ and C^*_{Ar} represent equilibrium concentrations of inert atmospheric gases at 1 bar and temperature T, while $C_{O_2,\mathrm{meas}}$ denotes the measured dissolved oxygen concentration in raw groundwater.From a thermodynamic standpoint, supersaturation in DAF arises from the rapid reduction in the partial pressure of the injected gas phase. Since methane is not re-pressurized in the saturator and does not experience an imposed pressure gradient during recycle pressurization, it does not contribute to the calculated supersaturation ratio S.

The supersaturation ratios reported in this study reflect the effective supersaturation achieved in the flotation jar after mixing pressurized whitewater with raw groundwater, rather than the theoretical supersaturation expected from complete pressure release. For the investigated operating conditions, the concentration-based definition of supersaturation is numerically consistent with the effective supersaturation expressed by Equation (4).

$$S_{eff} = 1 + R(P_{abs} - 1) \quad (4)$$

where S_{eff} is the effective supersaturation ratio in the flotation jar, accounting for incomplete pressure release due to dilution with raw water; R(–) is the recycle ratio, defined as the volumetric fraction of pressurized whitewater relative to the total flow in the flotation jar; P_{abs} is the absolute pressure of the pressurized whitewater prior to release, expressed in bar; the value 1 bar represents atmospheric pressure, such that $(P_{\text{abs}} - 1)$ corresponds to the effective pressure drop driving gas release.

2.5. Microbubble Dynamics and Bubble–Floc Interactions

Microbubble rise velocities in the 20–100 μm size range can be reasonably approximated using Stokes' law under low-Reynolds-number conditions typical of DAF systems [5,23]. In this regime, microbubbles remain nearly spherical and inertial effects are limited, allowing first-order estimation of terminal rise velocities. These hydrodynamic approximations provide a simplified and physically consistent basis for analyzing microbubble transport in low-turbidity groundwater systems.

Bubble–floc interactions are typically described using established flotation models that separate collision efficiency from attachment probability [24,25]. In this study, attachment probability is interpreted within the DLVO framework (Derjaguin–Landau–Verwey–Overbeek theory), which represents bubble–floc interactions as a balance between attractive van der Waals forces and electrostatic repulsion, thereby providing a mechanistic explanation for attachment behavior under coagulation–flotation conditions [10].

Supersaturation represents the thermodynamic driving force for gas release following depressurization and defines the conditions under which microbubble nucleation may occur in DAF systems. In this study, supersaturation was evaluated within a modeling framework and not determined from experimental DAF operation. The supersaturation ratio (S) was defined as the ratio between the dissolved-air concentration under pressurized conditions and the baseline dissolved-air concentration in raw groundwater, following the approach described by [4] (Equation (5)):

$$S = \frac{C_{\text{press}}}{C_{\text{ambient}}} \quad (5)$$

where C_{press} is the equilibrium dissolved-air concentration at the applied operating pressure and temperature, and C_{ambient} represents the groundwater-specific baseline dissolved-air concentration prior to pressurization.

Microbubble nucleation was assessed using an indicative supersaturation range ($S \approx 1.3$–1.5), consistent with values generally required for heterogeneous bubble nucleation in aqueous systems [5,26,27]. In the present work, this range was used as a reference criterion to evaluate whether the modeled thermodynamic conditions were sufficient to promote spontaneous microbubble formation, rather than as a direct prediction of bubble nucleation behavior. The amount of gas potentially available for microbubble formation was estimated from the calculated excess dissolved-air concentration released during pressure reduction from pressurized to near-atmospheric conditions. No direct measurement of bubble number or size was performed.

Because dissolved-air flotation was not experimentally conducted, effective supersaturation was evaluated conceptually by accounting for the recycle ratio R, defined as the ratio of pressurized, air-saturated water volume V_{SW} to the effective system volume. The recycling ratio was defined following standard DAF jar-test procedures provided by the equipment manufacturer [14] (Equation (6)):

$$R = \frac{V_{SW}}{V_J - V_D} \tag{6}$$

where V_J is the total jar volume and V_D is the volume decanted prior to the introduction of pressurized water.

Supersaturation ratios reported in this study represent modeled, effective supersaturation conditions that would be expected after mixing pressurized whitewater with raw groundwater, rather than experimentally measured supersaturation values from laboratory DAF operation.

2.6. Bubble-Dynamics Modeling

2.6.1. Parametric Evaluation of Bubble Diameter

After microbubble nucleation, bubble diameter strongly influences flotation hydrodynamics and bubble–floc interactions. In the present study, a full bubble population balance or nucleation-kinetics derivation was not performed. Instead, bubble diameter was evaluated parametrically within physically realistic ranges consistent with calculated supersaturation levels and commonly reported DAF operating conditions.

Although the volumetric gas-release relationship (Equation (7)) illustrates the theoretical dependence of bubble diameter on released gas volume and nucleation-site density, the number of active nucleation sites (N_b) was not experimentally determined. Therefore, Equation (7) is presented as a scaling relationship rather than as a predictive derivation of an actual bubble size distribution [5]:

$$d_b = \left(\frac{6V_g}{\pi N_b}\right)^{1/3} \tag{7}$$

where V_g denotes the volume of gas released during depressurization and N_b represents the estimated number of nucleation sites.

Bubble diameter ranges were evaluated for the supersaturation conditions corresponding to each investigated pressure–temperature combination. As direct measurements of bubble diameters were not performed, a representative microbubble diameter range of 35–80 μm was adopted based on the literature-reported DAF performance windows [3,4]. This adopted range was used as a physically realistic basis for subsequent evaluation of bubble rise velocity and bubble–floc interaction efficiency under groundwater-specific operating conditions.

2.6.2. Terminal Rise Velocity

Following microbubble formation, their upward transport in the flotation zone is governed by the balance between buoyant forces and viscous resistance, which defines the terminal rise velocity. In the present study, bubble rise velocities were estimated within the adopted modeling framework, rather than experimentally measured.

For microbubbles under low-Reynolds-number conditions (Re < 1), the terminal rise velocity was calculated using Stokes' law (Equation (8)), which is applicable to spherical bubbles in laminar flow [5]:

$$v_t = \frac{2}{9}\frac{(\rho_w - \rho_g)gd_b^2}{\mu} \tag{8}$$

where v_t is the terminal rise velocity, ρ_w and ρ_g are the densities of water and gas, respectively, g is gravitational acceleration, d_b is the bubble diameter, and μ is the dynamic viscosity of water.

For larger bubbles, where inertial effects become non-negligible (Re > 1), terminal rise velocities were estimated using empirical drag correlations that extend beyond the Stokes regime. In this study, generalized formulations consistent with the Allen and Clift–Grace–Weber approaches were applied (Equation (9)) [5]:

$$v_t = \sqrt{\frac{4(\rho_w - \rho_g) g d_b}{3 \rho_w C_D}} \tag{9}$$

where C_D denotes the drag coefficient.

The Reynolds number (Equation (10)) was used to check whether the flow was mainly controlled by viscosity or by inertia. Based on this, the appropriate drag equation was chosen:

$$\mathrm{Re} = \frac{\rho_w v_t d_b}{\mu} \tag{10}$$

For intermediate Reynolds numbers, the adopted drag formulation provides a continuous transition between the Stokes and inertia-dominated regimes and is consistent with established Allen and Clift–Grace–Weber correlations for spherical bubbles.

Terminal rise velocities were evaluated for bubble diameters between 20 and 150 µm and for water temperatures representative of the groundwater source (13–17 °C). These modeled velocity ranges were subsequently used to assess bubble residence time and bubble–floc contact potential under groundwater-relevant flotation conditions.

2.6.3. Bubble–Floc Collision and Attachment Efficiencies

Collision Efficiency (Ec)

In dissolved-air flotation, effective separation requires that rising microbubbles physically encounter suspended flocs. This initial contact step was described using the collision efficiency (Ec), which represents the probability that a bubble moving through the water column will collide with a floc under flotation conditions.

In the present study, collision efficiency was estimated using a simplified analytical expression derived from classical flotation theory and widely applied in flotation modeling (Equation (11)) [9,24,25]:

$$E_c = \frac{3}{2}\left(\frac{d_b}{d_f + d_b}\right)^2 \tag{11}$$

where d_b is the bubble diameter and d_f is the characteristic floc diameter.

This formulation represents a geometric-interception approximation derived under creeping-flow and low-turbulence assumptions, where bubble–floc encounters are primarily governed by relative buoyancy-driven motion. The expression does not resolve hydrodynamic wake effects, turbulence-induced shear interactions, or trajectory deflection, but instead provides a first-order analytical estimate of encounter probability based on size ratio scaling. Consequently, Ec should be interpreted as a relative geometric collision indicator rather than as a fully resolved hydrodynamic capture probability.

This formulation captures the geometric nature of bubble–floc encounters, showing that collision probability increases with increasing bubble size, while larger floc diameters reduce the collision efficiency predicted by this geometric model (Equation (11)). The model assumes spherical particles, low turbulence, and relative motion governed primarily by buoyancy-driven bubble rise, conditions that are consistent with DAF operation in low-turbidity groundwater.

Floc diameters were not measured directly in this study but were defined based on the coagulation–flocculation conditions established in the jar-test series and on representative size ranges reported in the literature for ferric-based coagulation and polymer-assisted flocculation in groundwater and low-turbidity waters. Typical floc diameters in the range of 50–300 μm were therefore adopted for modeling purposes [3,4,28]. The estimated collision efficiency values were subsequently used as input parameters in the evaluation of overall bubble–floc interaction efficiency and flotation potential under groundwater-specific conditions.

To assess parameter sensitivity, collision efficiency was evaluated across the full modeled bubble diameter range (20–150 μm) and representative floc diameters (50–300 μm). The results demonstrate monotonic scaling behavior, where Ec increases with increasing bubble diameter and decreases with increasing floc diameter according to the geometric ratio term. Importantly, although absolute Ec values vary with assumed diameters, the relative ranking of coagulation regimes remains consistent across the evaluated parameter space. This indicates that the mechanistic interpretation of bubble–floc interaction trends is robust with respect to plausible uncertainty in bubble and floc size.

2.6.4. Bubble–Floc Attachment Efficiency (Ea)

Following a successful bubble–floc collision, flotation efficiency further depends on whether the bubble remains attached to the floc long enough to enable upward transport. This process was described using the attachment efficiency (Ea), which represents the probability that a collision results in stable bubble–floc adhesion. In this study, attachment efficiency was modeled using a Boltzmann-type probability expression, which relates the likelihood of attachment to the interfacial energy barrier separating the bubble and floc surfaces. This approach is consistent with DLVO-based descriptions of particle–bubble interactions commonly applied in flotation and colloid science [10]. (Equation (12)):

$$E_a = exp\left(-\frac{W}{kT}\right) \tag{12}$$

where W is the effective interaction energy barrier, k is the Boltzmann constant, and T is the absolute temperature.

In the present study, the interaction energy barrier W was not calculated from measured DLVO/EDLVO surface-chemical parameters (e.g., zeta potential, ionic strength, Hamaker constants, or specific adsorption energies). Instead, W was varied parametrically within physically plausible ranges to evaluate the sensitivity of flotation-relevant behavior to changes in surface interaction conditions. Accordingly, the reported Ea values should be interpreted as relative indicators of attachment propensity rather than as quantitatively resolved surface-force predictions.

The energy barrier W reflects the combined influence of floc surface charge, hydrophobicity, and polymer-mediated interactions [10]. In ferric-based coagulation systems, flocs are typically characterized by relatively hydrophilic surfaces and strong electrostatic repulsion, which can limit stable bubble attachment. In contrast, the addition of polyaluminum chloride (PAC) promotes polymer bridging and modifies surface chemistry, reducing repulsive forces and increasing the probability of sustained bubble–floc attachment.

Because $FeCl_3$- and $FeCl_3$/PAC-induced flocs differ in surface properties and structural compactness, attachment efficiency was treated as a key parameter governing overall flotation performance. Rather than being directly measured, attachment efficiency was explored parametrically to assess its influence on flotation behavior. Because the interfacial energy barrier W was not measured, E_a values were evaluated over representative

ranges consistent with reported surface-chemical conditions in ferric- and polymer-assisted coagulation systems.

Ferric coagulation and polymer-assisted coagulation are known to modify surface charge density, interfacial hydrophobicity, and electrostatic double-layer thickness. Although these effects were not quantified experimentally in the present work, the parametric variation in W provides a physically consistent way to explore how reduced electrostatic repulsion or enhanced polymer bridging may influence attachment probability. The objective was therefore to capture the directional influence of coagulation chemistry on flotation-relevant interactions rather than to compute absolute DLVO interaction energies.

2.7. Integration with Laboratory Pretreatment Data

Laboratory coagulation–flocculation experiments previously performed on the same groundwater matrix were used in this study to contextualize and interpret the results of the thermodynamic and bubble-dynamics modeling [13]. The present work does not repeat experimental flotation tests; instead, previously published jar-test outcomes were used to define realistic treatment conditions and to provide qualitative reference trends for comparison.

Aggregated removal trends for color, TOC, and arsenic obtained under different coagulation regimes were used as benchmark indicators of separation performance. These trends were not treated as direct DAF results, but rather as experimentally observed outcomes reflecting differences in floc formation, stability, and contaminant association under realistic pretreatment conditions.

Model predictions of gas solubility, supersaturation, microbubble size distribution, rise velocity, and bubble–floc interaction efficiencies were therefore evaluated in relation to these experimentally documented trends. This comparison enabled assessment of whether the modeled thermodynamic and hydrodynamic behavior is physically consistent with the pretreatment performance observed under optimized coagulation conditions. In this way, the integration of modeling and laboratory data provides a mechanistic interpretation of how coagulation chemistry and microbubble behavior jointly influence the potential effectiveness of dissolved-air flotation as a pretreatment step.

Coagulation Behavior Relevant for Flotation

Arsenic removal by ferric salts in drinking-water treatment is primarily governed by the formation of ferric hydroxide precipitates, which provide reactive surfaces for arsenic adsorption and inner-sphere complexation, particularly for oxidized arsenic species under typical treatment conditions [29]. The addition of PAC further enhances coagulation by promoting polymer bridging and floc strengthening, leading to the formation of larger, denser, and more structurally stable flocs [30].

In previously reported laboratory jar-test studies conducted on Zrenjanin groundwater, combined $FeCl_3$/PAC coagulation consistently resulted in improved removal of color, TOC, and particulate-bound arsenic compared with single-coagulant [13]. These outcomes indicate that coagulant composition strongly influences floc structure and surface properties, which are critical determinants of subsequent physical separation processes.

In the present study, these experimentally established coagulation regimes were not re-evaluated as treatment results but were used to define representative floc characteristics for modeling purposes. Specifically, $FeCl_3$/PAC-induced flocs were considered indicative of conditions most favorable for bubble–floc attachment and flotation and were therefore used as the basis for defining floc size ranges, density assumptions, and surface interaction properties applied in the bubble-dynamics modeling framework.

2.8. Limitations of the Modeling Approach

The modeling approach adopted in this study is deterministic and theoretical in nature, relying on the literature-based parameter ranges and physically consistent assumptions rather than direct flotation measurements. The work should therefore be interpreted as a feasibility and process-screening study rather than as an experimentally validated performance assessment.

A full derivation of bubble size distribution from nucleation kinetics and coalescence modeling was beyond the scope of this study. Bubble diameters were treated parametrically to evaluate hydrodynamic sensitivity, using ranges consistent with DAF design guidance and the literature rather than direct measurement. Collision and attachment metrics depend on uncertain inputs, including bubble diameter, floc size distribution, turbulence level, and surface-chemical interaction barriers. Although collision efficiency was evaluated over broad size ranges, the adopted formulation remains a simplified geometric approximation and does not account for turbulence-modified capture probabilities.

Attachment efficiency was evaluated parametrically because DLVO/EDLVO inputs (e.g., bubble and floc zeta potential, ionic strength, and Hamaker constants) were not measured for the studied groundwater matrix. A fully resolved DLVO/EDLVO interaction model would require experimentally determined surface potentials and material-specific constants, which were beyond the scope of the present study.

The groundwater contains elevated methane under reducing conditions; however, methane is not part of the pressurized "dissolved air" introduced by the saturator and lacks a defined gas-phase boundary condition in this framework. Its potential contribution was therefore treated separately as a bounded sensitivity case using Henry's-law constants rather than as a calibrated multicomponent gas-transfer model. Although dissolved methane may partially degas during pressure release depending on mass-transfer kinetics, a rigorous multicomponent gas-transfer model including methane stripping was beyond the scope of this study and represents a direction for future experimental validation.

Practical saturator pressures and bubble diameters vary across systems, and bubble size depends on release-device characteristics and coalescence behavior, further supporting the scenario-based treatment adopted in this work.

Figure 1 illustrates the conceptual dissolved-air flotation system represented within the present modeling framework. The schematic distinguishes between experimentally derived coagulation–flocculation inputs and the thermodynamic–hydrodynamic flotation processes evaluated analytically. The modeled configuration reflects a conventional DAF system consisting of a saturator, pressure-release device, contact zone, and separation tank operating under groundwater-specific conditions.

3. Results

Prior to presenting the results of the thermodynamic and bubble-dynamics modeling, the key input parameters and operating conditions adopted in the calculations are summarized to ensure transparency and reproducibility. All model inputs were derived from measured groundwater characteristics and realistic operating ranges relevant to DAF pretreatment at the Zrenjanin water treatment plant.

Groundwater temperature at the intake varied between 13 and 17 °C, reflecting stable seasonal conditions typical of the deep aquifer supplying the system. Pressurization levels of 4 and 6 bar (gauge) were selected to represent the lower and upper bounds of typical operating pressures reported for drinking-water DAF systems and applied in laboratory-scale DAF jar testers [3,4]. Absolute pressures used in thermodynamic calculations were obtained by adding atmospheric pressure (1 bar).

The raw groundwater exhibited strongly reducing conditions, with dissolved oxygen concentrations consistently below 0.5 mg/L and dissolved methane concentrations ranging from 12 to 21 mg/L [13]. These characteristics indicate that the groundwater is not in equilibrium with atmospheric air and therefore requires a groundwater-specific definition of baseline dissolved-gas conditions for supersaturation calculations.

Temperature-dependent water density and viscosity were assumed based on standard freshwater properties, while equilibrium gas solubility under pressure was calculated using Henry's law with appropriate temperature correction. These parameters formed the basis for subsequent calculations of equilibrium dissolved-air concentration, effective supersaturation ratio, expected microbubble size distribution, and bubble rise velocity.

The results presented represent model-based predictions of thermodynamic and bubble-dynamics behavior under conditions representative of Zrenjanin groundwater pretreatment and are interpreted in relation to experimentally observed coagulation–flocculation trends reported previously. The reported ranges correspond to operating conditions typical of pilot- and full-scale DAF units used in drinking-water treatment and should be interpreted as process-design screening parameters rather than laboratory-scale device simulations.

Detailed equations, modeling assumptions, temperature corrections, and step-by-step calculations underlying the reported ranges of gas solubility, supersaturation, predicted microbubble diameters, and bubble–floc interaction efficiencies are provided in the Supplementary Material to ensure full transparency and reproducibility of the modeling approach.

Pre-oxidation with sodium hypochlorite altered floc chemistry and was associated with the formation of disinfection by-products, as confirmed by measured THM concentrations in jar-test effluents. Across four jar-test series (JAR 1–4), consistent coagulation regimes were identified based on residual water-quality parameters and treatment responses, allowing the definition of representative floc conditions relevant for flotation modeling (Table 1). Ferric chloride applied alone resulted in moderate to dense flocs with partial arsenic removal, while pre-oxidation with sodium hypochlorite altered floc chemistry but was associated with the formation of disinfection by-products. In contrast, combined $FeCl_3$/PAC coagulation consistently produced compact, stable flocs with low residual arsenic, color, and TOC across all experimental series. These $FeCl_3$/PAC regimes were therefore selected as representative input conditions for the thermodynamic and bubble-dynamics modeling of dissolved-air flotation presented in the following sections.

Table 1. Condensed summary of representative coagulation regimes derived from four jar-test series (JAR 1–4).

Regime ID	Source JAR Series	$FeCl_3$ (mg/L)	PAC (mg/L)	NaOCl (mg/L)	Color (°Pt–Co)	TOC (mg C/L)	As (µg/L)	Turbidity (NTU)	Interpretation for DAF
RW	All	–	–	–	74–76	7.3–9.2	108–141	5–6	Raw groundwater (baseline)
F-M	JAR 1–2	20–30	–	–	77–91	7.8–9.4	73–89	5–7	Moderate Fe flocs, limited As binding
F-H	JAR 1–2	40–120	–	–	54–78	7.4–8.6	26–64	3–10	Dense Fe flocs, incomplete NOM removal

Table 1. *Cont.*

Regime ID	Source JAR Series	$FeCl_3$ (mg/L)	PAC (mg/L)	NaOCl (mg/L)	Color (°Pt–Co)	TOC (mg C/L)	As (µg/L)	Turbidity (NTU)	Interpretation for DAF
F-O	JAR 1–2	40–50	–	10–20	58–75	8.6–9.4	64–101	2–9	Oxidation-affected flocs; DBP formation observed (THMs detected)
F-P (opt)	JAR 1–4	20–25	20–30	–	11–33	3.1–5.3	<10–22	1.3–2.8	Dense, stable flocs optimal for DAF

Notes: Abbreviations in Table 1: Regime ID: RW—raw groundwater without chemical addition; F-M—moderate ferric chloride dosing; F-H—high ferric chloride dosing; F-O—ferric chloride dosing combined with sodium hypochlorite pre-oxidation; F-P—combined ferric chloride and polyaluminum chloride dosing (optimized coagulation regime); NOM—natural organic matter; DBPs—disinfection by-products; THMs—trihalomethanes.

The parameters summarized in Table 2 were either directly calculated from the thermodynamic results (Table 1) or adopted from the representative literature ranges to support subsequent modeling of microbubble behavior and bubble–floc interactions.

Table 2. Derived and literature-based parameters used for microbubble and bubble–floc interaction analysis.

Parameter	Symbol	Value/Range	Unit	Source/Basis
Groundwater temperature	T	13–17	°C	Measured seasonal values at Zrenjanin source
Operating pressure	P	4; 6	bar	Typical full-scale DAF operating range
Atmospheric pressure	P_0	1.0	bar	Standard condition
Dissolved oxygen (raw water)	DO	<0.5	mg/L	Field measurements (reducing conditions)
Dissolved methane	CH_4	12–21	mg/L	Field measurements
Water density	ρ_w	998–999	kg m^{-3}	Temperature-dependent freshwater properties
Dynamic viscosity of water	µ	(1.05–1.14) × 10^{-3}	Pa s	Temperature-dependent freshwater properties
Gas density (air)	ρ_g	1.18–1.25	kg m^{-3}	Standard air properties
Henry's constant for air (25 °C)	H_0	7.7 × 10^{-4}	mol m^{-3} Pa^{-1}	Literature value [4]
Temperature correction	—	Van't Hoff relation	—	Section 2.2
Supersaturation ratio	S	1.35–1.89	—	Calculated (this study)
Target microbubble diameter	d_b	35–80	µm	Typical DAF microbubble range [14]
Floc diameter ($FeCl_3$/PAC)	d_f	100–300	µm	Estimated from coagulation conditions
Gravitational acceleration	g	9.81	m s^{-2}	Constant

Equilibrium dissolved-air concentrations C_{press} were calculated using Henry's law with temperature correction. The dependence of dissolved-air solubility on temperature and operating pressure is illustrated in Figure 2, which provides the thermodynamic basis for defining supersaturation conditions relevant to DAF operation. The supersaturation ratio, defined as $S = C_{press}/C_{ambient}$, represents the groundwater-specific baseline

dissolved-air concentration defined in Section 2.2. Methane was not included in the supersaturation calculation but was used to characterize reducing source conditions.

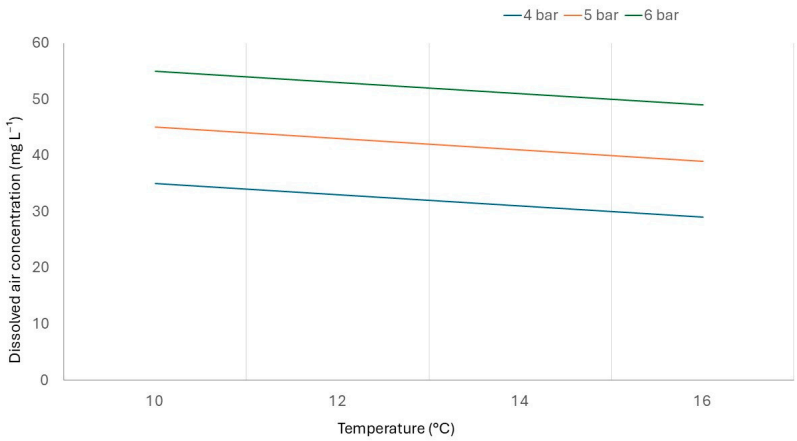

Figure 2. Modeled gas solubility of dissolved air as a function of temperature at operating pressures of 4, 5, and 6 bar.

3.1. Thermodynamic Calculations of Gas Solubility

Thermodynamic calculations were performed at the boundary combinations of the investigated pressure–temperature range in order to capture the minimum and maximum expected levels of gas dissolution and effective supersaturation under realistic operating conditions. As expected, equilibrium dissolved-air concentration increased with increasing pressure and decreased with increasing temperature within the investigated groundwater temperature range (13–17 °C).

At 6 bar (gauge) and 13 °C, the equilibrium dissolved-air concentration introduced via pressurization was approximately 1.4 times higher than that obtained at 4 bar and 17 °C. The calculated conditions resulted in effective supersaturation ratios S_{eff} ranging from 1.35 to 1.89, which exceed values commonly associated with the onset of spontaneous microbubble nucleation in dissolved-air flotation systems. Table 3 summarizes the effective dissolved-air concentrations and corresponding supersaturation ratios calculated for the investigated operating conditions.

Table 3. Effective dissolved-air concentration and supersaturation ratios at relevant DAF operating conditions.

Pressure (bar)	Temperature (°C)	Effective Dissolved-Air Concentration After Mixing, C_{eff} (mg/L) *	S_{eff}
4	17	29–31	1.35
4	13	33–35	1.47
6	17	39–41	1.72
6	13	43–46	1.89

Notes: * C_{eff} denotes the effective dissolved-air concentration in the flotation jar after mixing pressurized whitewater with raw groundwater. Supersaturation ratios were calculated using Equation (5), with the recycling ratio defined according to the jar-test procedure [14].

In the present calculations, the baseline dissolved-gas concentration prior to pressurization $C_{ambient}$ was defined as a groundwater-specific reference value, accounting for the measured dissolved oxygen concentration (<0.5 mg/L) and equilibrium concentrations of inert atmospheric gases (primarily N_2 and Ar) at 1 bar and the corresponding water temperature. These results indicate that the groundwater temperature range characteristic of the Zrenjanin source (13–17 °C) is favorable for achieving sufficient effective gas

supersaturation, thereby enabling stable microbubble release upon depressurization. The thermodynamic conditions of the groundwater investigated are therefore compatible with efficient dissolved-air flotation pretreatment.

3.2. Predicted Microbubble Size Distribution

Lower groundwater temperature and higher operating pressure are expected to favor the formation of smaller microbubbles due to increased effective gas supersaturation. Based on the calculated supersaturation ratios $S_{eff} = 1.35–1.89$ and representative microbubble size ranges reported for efficient dissolved-air flotation operation, the expected bubble diameters under the investigated conditions were estimated to fall within the following ranges: 60–90 μm (4 bar, 17 °C), 50–80 μm (4 bar, 13 °C), 40–70 μm (6 bar, 17 °C), and 35–60 μm (6 bar, 13 °C) (Figure 3).

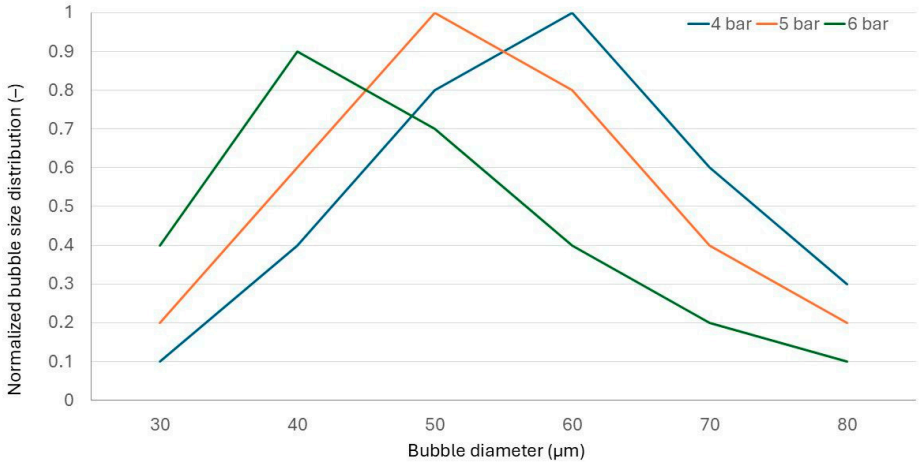

Figure 3. Predicted microbubble size distributions under different pressurization pressures (4, 5, and 6 bar) for groundwater DAF pretreatment.

The smallest predicted bubble diameters were associated with the highest pressure and lowest temperature conditions, which provide the most favorable thermodynamic environment for gas release and microbubble formation. These predicted size ranges are consistent with microbubble diameters commonly reported for optimized full-scale and pilot-scale DAF systems treating low-turbidity waters, as summarized in the literature [3,4,6].

3.3. Terminal Rise Velocity of Microbubbles

The terminal rise velocity increased with increasing bubble diameter, consistent with the quadratic dependence predicted by Stokes' law under low-Reynolds-number conditions. For bubble diameters in the range of 35–60 μm, predicted velocities were approximately 2.2–7.3 mm s^{-1}, while bubbles of 60–90 μm exhibited velocities of 6.5–16.3 mm s^{-1}. These values represent upper-bound estimates under ideal creeping-flow conditions. Stokes-law calculations presented in Table S2 provide theoretical upper-bound estimates for terminal rise velocity under creeping-flow conditions. However, microbubbles in practical DAF systems frequently operate at Reynolds numbers approaching or exceeding unity, where increased drag and flow separation reduce rise velocities below Stokes predictions. Consequently, the velocity ranges reported in the Results represent more physically realistic estimates under actual operating conditions.

For bubble diameters exceeding approximately 100 μm, inertial effects can no longer be neglected, and bubble motion cannot be adequately described by ideal Stokes behavior. As a result, rise velocities are better represented by empirical correlations developed for transitional flow regimes.

The predicted rise velocities indicate that typical hydraulic residence times in DAF systems (on the order of 10–20 min) are sufficient to allow upward transport and separation of microbubbles under the investigated conditions. Smaller microbubbles generated under lower temperatures and higher pressures are therefore expected to remain in the flotation zone for longer periods, which favors bubble–floc contact and attachment. This behavior is particularly relevant for the flotation removal of NOM-associated and arsenic-bearing flocs in low-turbidity groundwater systems.

3.4. Bubble–Floc Interaction Efficiency

3.4.1. Collision Efficiency (Ec)

Collision efficiency E_c was found to increase with decreasing bubble diameter and increasing floc size, consistent with classical flotation theory. Coagulation regimes involving ferric chloride combined with PAC produced flocs with larger effective diameters and more compact structures compared with single-coagulant systems. Accordingly, the combined $FeCl_3$/PAC system yielded the highest estimated collision efficiency within the modeled range, relative to single-coagulant configurations (Figure 4).

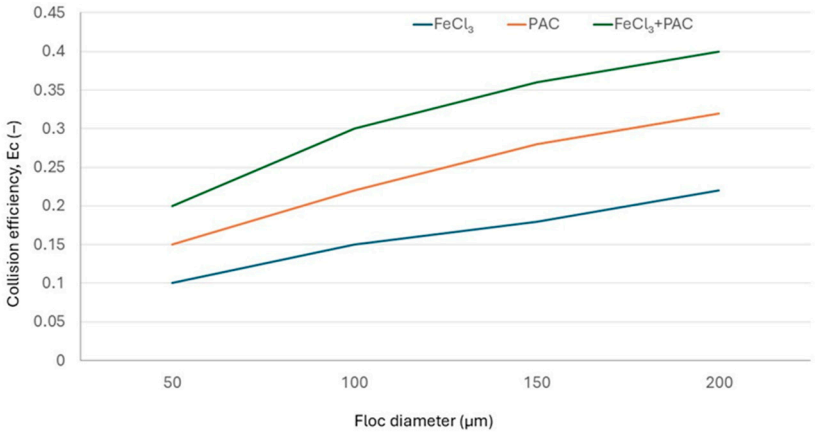

Figure 4. Modeled collision efficiency (Ec) between microbubbles and coagulated flocs as a function of floc diameter for different coagulation regimes.

In this study, collision efficiency was evaluated using the Yoon–Luttrell model, with bubble and floc size ranges informed by jar-test observations and the literature values. As such, the reported efficiencies represent theoretical estimates rather than direct measurements.

Based on the representative ranges of microbubble diameters (35–90 μm) and floc sizes (approximately 100–300 μm), collision efficiencies calculated using the Yoon–Luttrell model span broad ranges (Table S4). Subranges of these values, qualitatively consistent with observed differences in floc structure from jar tests, correspond to approximately 0.19–0.31 for $FeCl_3$-only systems, 0.22–0.36 for PAC-assisted systems, and 0.34–0.47 for the combined $FeCl_3$ + PAC configuration. The higher collision efficiencies predicted for the combined $FeCl_3$/PAC regime reflect the formation of larger and denser flocs, which is consistent with experimentally observed improvements in color and arsenic removal reported in previous laboratory pretreatment studies. These results indicate that optimized coagulation conditions significantly enhance the probability of bubble–floc encounters under flotation-relevant conditions.

3.4.2. Attachment Efficiency (Ea)

Modeled attachment efficiency reflects the influence of floc surface properties and chemistry on bubble–floc adhesion. Sensitivity analysis of the Boltzmann-type attachment model (Figure 5) indicates that lower interfacial energy barriers correspond to higher attach-

ment efficiencies. In this context, $FeCl_3$-only systems are expected to exhibit relatively lower attachment probabilities, while PAC-assisted and combined $FeCl_3$ + PAC systems are associated with progressively higher attachment efficiencies, consistent with polymer bridging and reduced energy barriers. Representative attachment-efficiency ranges corresponding to these trends are illustrated in Figure 5.

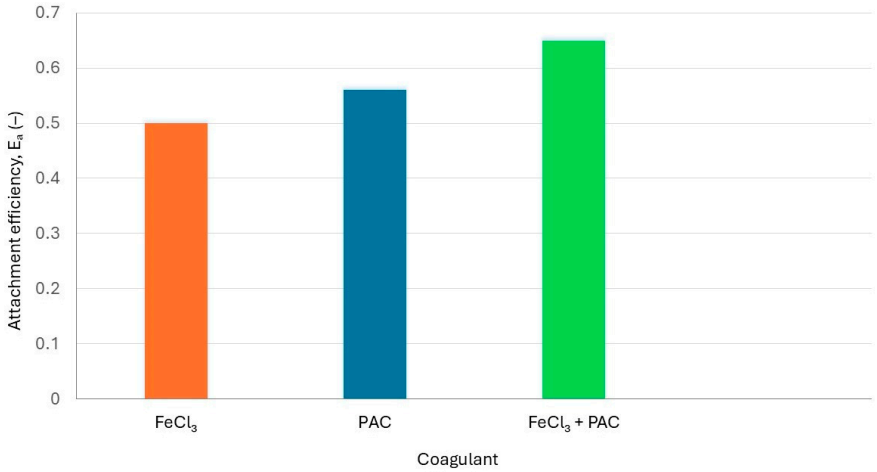

Figure 5. Modeled attachment efficiency (Ea) of microbubbles to flocs formed under different coagulation regimes.

3.5. Integration of Model Predictions with Laboratory Observations

Although no new dissolved-air flotation experiments were conducted, previously published coagulation–flocculation results for the same groundwater were used solely to support qualitative interpretation of relative trends predicted by the modeling framework. The thermodynamic and bubble-dynamics modeling framework developed here was therefore evaluated against experimentally observed pretreatment trends rather than direct flotation performance.

Model predictions reproduced the key tendencies reported in laboratory studies. In particular, the smallest estimated microbubble diameters (approximately 35–60 μm) were associated with pressure–temperature conditions under which enhanced removal of color and total organic carbon was previously achieved. Higher modeled collision and attachment efficiencies for the combined $FeCl_3$ + PAC coagulation regime are consistent with experimentally observed improvements in the removal of particulate-bound arsenic reported in previous laboratory studies [13].

Predicted terminal rise velocities confirmed that the clarification times observed in laboratory pretreatment tests are physically compatible with typical dissolved-air flotation hydrodynamics. Taken together, the qualitative agreement between modeled bubble behavior and previously observed treatment outcomes supports the relevance of the proposed mechanistic framework for interpreting and predicting DAF performance in complex groundwater systems.

4. Discussion

The thermodynamic and bubble-dynamics analysis provides important practical implications for the design and operation of DAF systems treating cold, arsenic-rich groundwater. It is important to note that dissolved-air flotation is not proposed here as a universal replacement for established groundwater treatment technologies such as adsorption, ion exchange, or membrane filtration. Rather, the present analysis positions DAF as a complementary pretreatment option under conditions where coagulation effectively transfers dissolved arsenic and NOM into separable particulate forms. In such systems, flotation

may reduce hydraulic loading on downstream filtration units, improve sludge characteristics compared with sedimentation, and provide enhanced removal of low-density organic flocs that are not efficiently captured by gravity clarification alone. The relative advantage of DAF therefore depends on site-specific hydrochemistry, treatment objectives, and integration within the overall process train. For groundwater temperatures in the range of 13–17 °C, moderate-to-high saturation pressures (5–6 bar gauge) are required to ensure stable microbubble formation under reducing hydrochemical conditions. The analysis further demonstrates that relatively small seasonal temperature variations can significantly influence DAF-relevant parameters. A decrease in temperature from 17 to 13 °C increases effective gas supersaturation by approximately 10–15%, leading to a shift in predicted microbubble diameters from roughly 60–90 µm to 35–60 µm under otherwise identical operating conditions. This pronounced temperature sensitivity indicates a potential seasonal influence on flotation performance that is rarely quantified for groundwater DAF systems but has direct implications for process robustness. The predicted optimal microbubble diameters therefore fall within the range of 35–70 µm, consistent with efficient bubble–floc interaction regimes derived from the modeling. In addition, the coagulation regime plays a critical role, as combined $FeCl_3$/PAC dosing produces the floc characteristics most favorable for flotation. These findings demonstrate that flotation efficiency cannot be considered independently of coagulation chemistry and saturator operating conditions, but rather as an integrated process governed by coupled thermodynamic and physicochemical constraints, as conceptually illustrated in Figure 6.

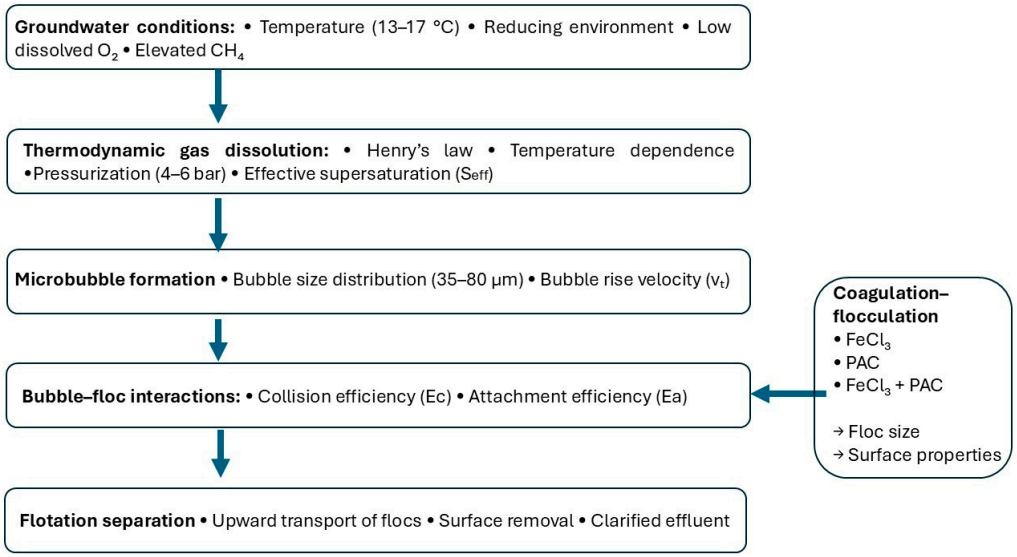

Figure 6. Conceptual framework linking thermodynamic conditions, microbubble dynamics, and bubble–floc interaction mechanisms in dissolved-air flotation pretreatment of groundwater.

The thermodynamic framework presented in this study provides a mechanistic interpretation of pretreatment behavior previously observed during laboratory coagulation–flocculation experiments on arsenic-rich groundwater. While much of the existing DAF literature focuses on surface waters with high turbidity or algal content, the same physical principles governing gas dissolution, supersaturation-driven microbubble formation, and bubble–floc interactions remain applicable to groundwater systems when temperature, pressure, and coagulation chemistry are jointly considered [3,4]. The modeled microbubble size ranges and interaction regimes are consistent with values reported for efficient DAF operation in drinking-water treatment, supporting the relevance of the proposed framework for groundwater applications.

Analysis of bubble–floc interactions further explain the superior performance of combined $FeCl_3$ and PAC coagulation observed in laboratory pretreatment studies. Compared with single-coagulant systems, $FeCl_3$ + PAC treatment promotes the formation of larger, denser, and mechanically more stable flocs, consistent with established coagulation and polymer-bridging theory [3,4,13]. Larger flocs increase the probability of collision with rising bubbles, whereas polymer-assisted coagulation enhances bubble–floc attachment through the modification of floc surface properties [3,4].

For arsenic removal specifically, the results emphasize that flotation effectiveness is contingent upon prior conversion of dissolved arsenic into particulate or co-precipitated forms capable of bubble attachment. Ferric coagulation removes arsenate primarily through adsorption and co-precipitation with iron (hydr)oxides via well-established surface-complexation mechanisms [11,12]. Natural organic matter can further influence arsenic partitioning by promoting Fe–As interactions mediated by dissolved organic matter (DOM), thereby affecting floc structure and separability [12,31]. These interactions indicate that favorable microbubble conditions alone are insufficient when coagulation is inadequate; effective oxidation and coagulation upstream of flotation are required to form flocs that can be separated by DAF.

Comparison of model-derived trends with previously published laboratory pretreatment results supports the relevance of the proposed mechanistic framework. Although direct measurements of bubble size and rise velocity were not available, the qualitative agreement between predicted microbubble behavior, bubble–floc interaction efficiencies and observed removal trends suggests that thermodynamic conditions and hydrodynamic interaction mechanisms are dominant drivers of flotation-related performance, rather than coagulant selection alone. In this respect, the present work complements empirical optimization studies by providing a physical–chemical rationale for observed treatment trends and for the robustness of certain coagulant–polymer strategies under variable groundwater conditions [3,4,31].

From a practical perspective, the findings suggest that DAF systems treating cold, arsenic-rich groundwater may benefit from operation at moderately elevated saturation pressures combined with coagulation regimes that promote dense and stable floc formation. The analysis also indicates that seasonal groundwater temperature variability may influence effective supersaturation and bubble characteristics, underscoring the potential value of adaptive operational control and jar-test-informed coagulation optimization in full-scale applications. Overall, this work offers a mechanistic framework for interpreting DAF pretreatment in chemically complex groundwater, linking thermo dynamics, bubble dynamics, and coagulation chemistry to enable a more predictive process design than empirical trial-and-error approaches. From an engineering perspective, the framework can be applied during preliminary design or retrofit evaluation of groundwater DAF systems. By defining pressure–temperature operating windows and bubble–floc interaction regimes, the model assists in selecting saturation pressure, recycle ratio, and coagulation strategy prior to pilot testing. It is not intended to replace pilot validation but to reduce uncertainty during process conceptualization.

5. Conclusions

Beyond its immediate application to the studied groundwater system, the proposed framework provides a transferable methodology for evaluating DAF pretreatment under non-ideal conditions, where conventional surface-water assumptions regarding dissolved gases and floc properties are not valid.

This study developed a mechanistic framework for interpreting the potential role of DAF as a pretreatment step for chemically complex, arsenic-rich, organic rich groundwater

with emphasized color. By integrating thermodynamic modeling of gas dissolution with bubble-dynamics analysis and previously published coagulation–flocculation data, the work provides a physically and chemically grounded explanation of how temperature, pressure, and floc properties jointly influence flotation-relevant behavior in groundwater systems.

Thermodynamic analysis demonstrated that groundwater temperatures typical of deep aquifers (13–17 °C) favor increased gas solubility under pressurization, resulting in effective supersaturation levels sufficient to support stable microbubble formation upon pressure release. Modeled bubble-dynamics results indicate that microbubbles formed under these conditions are expected to fall within size and rise-velocity ranges widely reported as optimal for flotation-based separation. The analysis further showed that coagulation regimes involving combined ferric chloride and polyaluminum chloride dosing produce flocs with properties most favorable for bubble–floc collision and attachment, providing a mechanistic explanation for the superior removal of color, natural organic matter, and particulate-bound arsenic observed in laboratory pretreatment studies.

The modeling results provide a mechanistic interpretation of previously observed coagulation behavior and indicate thermodynamically plausible conditions under which DAF could operate effectively. However, direct experimental flotation validation remains necessary to quantify actual removal efficiencies. The results demonstrate that flotation performance cannot be evaluated independently of upstream coagulation and that effective DAF design for groundwater requires integrated consideration of chemical speciation, floc formation, and gas dissolution behavior.

Building on these findings, ongoing work at the Zrenjanin water treatment plant includes pilot- and full-scale operational trials in which key thermodynamic parameters, such as saturation pressure, recycle ratio, and operating temperature, are systematically varied under real process conditions. The outcomes of these experiments will provide direct experimental validation of the modeled relationships presented here and will be reported in future publications. Together, the present study and forthcoming experimental results aim to support more predictive, mechanism-based optimization of DAF pretreatment for challenging groundwater matrices.

Supplementary Materials: The following supporting information can be downloaded at: https://www.mdpi.com/article/10.3390/w18050633/s1.

Author Contributions: Conceptualization, M.P. and Z.R.; methodology, M.K., I.R. and Z.R.; formal analysis, Z.R. and M.P.; investigation, M.K., I.R. and Z. R; resources B.C. and D.M.; writing—original draft preparation, M.P.; writing—review and editing, M.K. and Z.R.; visualization, B.C. and D.M.; supervision, M.K. and I.R. All authors have read and agreed to the published version of the manuscript.

Funding: This research received no external funding.

Data Availability Statement: The data supporting the findings of this study are contained within the article. The modeling parameters were derived from the literature sources and from laboratory coagulation–flocculation results described in the manuscript. No additional datasets were generated during the study.

Conflicts of Interest: The authors declare no conflicts of interest.

References

1. Dimkić, M.; Brauch, H.J.; Kavanaugh, M. *Groundwater Management in Large River Basins*; IWA Publishing: London, UK, 2008. [CrossRef]
2. Perović, M.; Obradović, V.; Zuber-Radenković, V.; Knöller, K.; Mitrinović, D.; Ćepić, Z. The Comprehensive Evaluation of Nitrate Origin and Transformation Pathways in the Oxic Alluvial Aquifer in Serbia. *Environ. Sci. Pollut. Res.* **2024**, *31*, 33030–33046. [CrossRef]
3. Edzwald, J.K. Dissolved Air Flotation and Me. *Water Res.* **2010**, *44*, 2077–2106. [CrossRef]

4. Edzwald, J.K.; Haarhoff, J. *Dissolved Air Flotation for Water Clarification*; McGraw-Hill: New York, NY, USA, 2012.
5. Clift, R.; Grace, J.R.; Weber, M.E. *Bubbles, Drops, and Particles*; Academic Press: New York, NY, USA, 1978.
6. Rubio, J.; Souza, M.L.; Smith, R.W. Overview of Flotation as a Wastewater Treatment Technique. *Miner. Eng.* **2002**, *15*, 139–155. [CrossRef]
7. Sander, R. Compilation of Henry's Law Constants (Version 4.0). *Atmos. Chem. Phys.* **2015**, *15*, 4399–4981. [CrossRef]
8. Atkins, P.; de Paula, J. *Physical Chemistry*, 8th ed.; Oxford University Press: Oxford, UK, 2006.
9. Schulze, H.J. Hydrodynamics of Particle–Bubble Interactions. *Miner. Process. Extr. Metall. Rev.* **1992**, *10*, 27–57. [CrossRef]
10. Israelachvili, J.N. *Intermolecular and Surface Forces*, 3rd ed.; Academic Press: London, UK, 2011.
11. Smedley, P.L.; Kinniburgh, D.G. A Review of the Source, Behaviour and Distribution of Arsenic in Natural Waters. *Appl. Geochem.* **2002**, *17*, 517–568. [CrossRef]
12. Hering, J.G.; Chen, P.-Y.; Wilkie, J.A.; Elimelech, M. Arsenic Removal from Drinking Water during Coagulation. *J. Am. Water Works Assoc.* **1996**, *88*, 155–167. [CrossRef]
13. Radibratović, Z.Z.; Cakić, B.B.; Kijevčanin, M.Lj.; Radović, I.R.; Mitrinović, D.M. Application Possibilities and Expected Effects of Dissolved Air Flotation in Groundwater Treatment for Removing TOC, Color and As. *Appl. Sci.* **2025**, *15*, 11255. [CrossRef]
14. Platypus Jar Tester Pty Ltd. *Platypus DAF Jar Tester: Instruction Manual*; Platypus Jar Tester: Southbank, Australia, 2019.
15. Jovanović, D.D.; Paunović, K.; Manojlović, D.D.; Jakovljević, B.; Rašić-Milutinović, Z.; Dojčinović, B.P. Arsenic in Drinking Water and Acute Coronary Syndrome in Zrenjanin Municipality, Serbia. *Environ. Res.* **2012**, *117*, 75–82. [CrossRef]
16. Agbaba, J.; Nikić, J.; Watson, M.; Tubić, A.; Kragulj Isakovski, M.; Maletić, S.; Dalmacija, B. Arsenic Removal from Groundwater by In-Line Coagulation. In *Proceedings of the 27th International Conference Ecological Truth and Environmental Research—EcoTER'19*; Technical Faculty in Bor, University of Belgrade: Bor, Serbia, 2019; pp. 258–263, ISBN 978-86-6305-097-6.
17. Agbaba, J.; Watson, M.; Kragulj Isakovski, M.; Stankov, U.; Dalmacija, B.; Tubić, A. Water Supply Systems for Settlements with Arsenic-Contaminated Groundwater—Making the Right Choice. *Appl. Sci.* **2023**, *13*, 9557. [CrossRef]
18. European Union. Directive (EU) 2020/2184 of the European Parliament and of the Council on the Quality of Water Intended for Human Consumption. *Off. J. Eur. Union* **2020**, *L435*, 1–62.
19. U.S. Environmental Protection Agency. National Primary Drinking Water Regulations; Arsenic and Clarifications to Compliance and New Source Contaminants Monitoring. *Fed. Regist.* **2001**, *66*, 6976–7066.
20. Republic of Serbia, Ministry of Health. *Pravilnik o higijenskoj ispravnosti vode za piće (Regulation on Hygienic Quality of Drinking Water)*; Official Gazette of the Republic of Serbia, No. 42/2019; Republic of Serbia, Ministry of Health: Belgrade, Serbia, 2019.
21. Han, M.; Kim, T.; Kim, J. Effects of Floc and Bubble Size on the Efficiency of the Dissolved Air Flotation (DAF) Process. *Water Sci. Technol.* **2007**, *56*, 109–115. [CrossRef]
22. Kaltchev, R. Fundamentals of Dissolved Air Flotation. In *Dissolved Air Flotation*; Springer Water; Springer: Cham, Switzerland, 2024; pp. 1–41.
23. Stokes, G.G. On the Effect of the Internal Friction of Fluids on the Motion of Pendulums. *Trans. Camb. Philos. Soc.* **1851**, *9*, 8–106.
24. Ralston, J. Controlled flotation processes: Prediction and manipulation of bubble–particle capture. *J. South Afr. Inst. Min. Metall.* **1999**, *99*, 27–34.
25. Nguyen, A.V.; Schulze, H.J. *Colloidal Science of Flotation*; CRC Press: Boca Raton, FL, USA; Taylor & Francis: Abingdon, UK, 2004.
26. Kosior, D. Bubble Formation and Motion in Liquids—A Review. *Minerals* **2023**, *13*, 1130. [CrossRef]
27. Jones, S.F. Bubble Nucleation from Gas Cavities—A Review. *Adv. Colloid Interface Sci.* **1999**, *80*, 27–50. [CrossRef]
28. Gregory, J. Optical monitoring of particle aggregates. *J. Environ. Sci.* **2009**, *21*, 2–7. [CrossRef]
29. Cui, L.; Li, Z.; Ding, J.; Huang, X.; Zhou, X.; Zheng, Z.; Cui, H.; Huang, C.; Xiang, L.; Huang, Y.; et al. Arsenate Adsorption, Desorption, and Re-adsorption on Fe–Mn Binary Oxides: Impact of Co-existing Ions. *Desalin. Water Treat.* **2024**, *320*, 100678. [CrossRef]
30. Bolto, B.; Gregory, J. Organic Polyelectrolytes in Water Treatment. *Water Res.* **2007**, *41*, 2301–2324. [CrossRef]
31. Duan, J.; Gregory, J. Coagulation by Hydrolyzing Metal Salts. *Adv. Colloid Interface Sci.* **2003**, *100–102*, 475–502. [CrossRef]